Divacancy in silicon: Hyperfine interactions from electron-nuclear double-resonance measurements. 2

Sieverts, E.G.; Ammerlaan, C.A.J.; Muller, S.H.

DOI
10.1103/PhysRevB.18.6834

Publication date
1978

Published in
Physical Review. B, Condensed Matter

PHYSICAL REVIEW B VOLUME 18, NUMBER 12 15 DECEMBER 1978

Divacancy in silicon: Hyperfine interactions from electron-nuclear double-resonance measurements. II

E. G. Sieverts,* S. H. Muller, and C. A. J. Ammerlaan
Natuurkundig Laboratorium der Universiteit van Amsterdam, Valckenierstraat 65, 1018 XE Amsterdam, The Netherlands
(Received 12 June 1978)

The Si-*G*7 EPR spectrum, which is attributed to the negative charge state of the divacancy in silicon, was investigated by electron-nuclear double resonance. Hyperfine interactions between the unpaired defect electron and various ^{29}Si nuclei were determined to obtain detailed information about the electron wave function. A total number of 33 hyperfine tensors was determined, of which 20 belong to a general class shell of atoms and 13 to a mirrorplane class shell. In this way the divacancy electron was probed in a region containing more than 100 lattice sites around the defect. Most hyperfine tensors exhibited approximate axial symmetry, a majority of these having their axial direction along a ⟨111⟩ crystal bond direction. An analysis of the interactions is given, using a wave function that is a linear combination of atomic orbitals. From a further theoretical approach of the defect wave function, using extended Hückel theory, preliminary results are given. In their discussion data from the positive divacancy are also included. In agreement with previous conclusions, the largest general class and mirrorplane class interactions were identified with the nearest-neighbor shells of both types. Further matching between hyperfine tensors and specific shells of lattice sites could not yet be made.

I. INTRODUCTION

This paper is the second in a series presenting results from electron-nuclear double resonance (ENDOR) experiments on the divacancy in silicon. The first paper[1] in this text further denoted by I was concerned with the positive charge state, this paper with the negative charge state of the divacancy. For some introductory remarks and general considerations about the divacancy we refer to I.

From all defects which can be produced in silicon by irradiation with energetic particles, the divacancy (V_2) is one of the best known. Contrary to simpler defects like the monovacancy or the self-interstitial, the divacancy is stable at room temperature. Divacancies can easily be produced by electron irradiation of silicon at room temperature. The divacancy is one of the first defects in silicon for which electron paramagnetic resonance (EPR) spectra could be identified with a high degree of reliability.[2-6] The spectra labeled Si-*G*6 and Si-*G*7 were derived to originate from the singly positive and the singly negative charge state of the divacancy, both of which constitute a $S=\frac{1}{2}$ paramagnetic center due to a single unpaired electron spin. Which charge state, ranging from singly positive to doubly negative, the divacancy assumes primarily depends on the position of the Fermi level. Several studies of the divacancy using EPR have been reported.[2-9] Also data from infrared absorption studies[10,11] and photoconductivity experiments[12] are known. Additional information about the energy levels associated with the different charge states of the divacancy originates from optical[13,14] and capacitance transient spectroscopy[15-17] studies. Both in I and in this paper we rely heavily upon the detailed information obtained by Watkins and Corbett.[5]

An important feature of many defects in silicon are the hyperfine interactions between the unpaired defect electron and neighboring magnetic ^{29}Si nuclei. For the negative divacancy V_2^- the three largest hyperfine interactions can be observed with EPR. Two of them have been reported before,[5] only the largest interaction, which will be labeled *M*1 in this paper, is well resolved. Weaker interactions cannot be observed with EPR. They are the origin of the inhomogeneous line broadening in the EPR spectrum. Using electron-nuclear double resonance a large part of these interactions can easily be resolved, however.

The importance of hyperfine interactions is due to the fact that they directly reflect the distribution of the wave function of the unpaired resonance electron. A hyperfine interaction can be expressed as a tensor whose isotropic part is the Fermi contact interaction which is proportional to the probability density of the electron on the relevant nuclear site. The anisotropic part is due to dipole-dipole interaction between the electronic and nuclear magnetic moments.

An ENDOR study of the shallow donors P, As, and Sb in silicon has produced an abundant number of hyperfine interactions.[18,19] That study formed a severe test for the effective-mass treatment[20-22] and the onset for an extension of this theoretical method in which good agreement between theoretical wave functions and observed hyperfine constants could be achieved.[23,24] For deep levels,

like most defects in silicon, no such promising theory was available, except perhaps extended Hückel theory (EHT).[25,26] ENDOR results for the positive divacancy V_2^+ presented in I, could not be compared with an EHT calculation by Lee and McGill.[27] Since then calculations especially intended for a description of experimental hyperfine interactions have been performed.[28-30] From these calculations for V_2^+ a rather satisfactory description of the defect wave function could only be given for the six nearest neighbors of the defect. For the remaining hyperfine interactions with more than 50 other neighbors a matching with a theoretical wave function turned out to be still impossible. For the present study on V_2^- results of a similar calculation are given.

II. EXPERIMENT

Experiments were performed on floating zone (FZ) single crystalline silicon specified to be dislocation free. Two kinds of phosphorus-doped n-type samples have been used which had preirradiation room-temperature resistivities of 0.34 and 0.03 Ω cm. Sample preparation and irradiation were as described in I. Samples were cut and ground to a roughly cylindrical shape with a length of 20 mm and a diameter of 2 mm, having a ⟨110⟩ crystal direction parallel to the long edges. Irradiation with 1.5-MeV electrons took place at temperatures not above 60 °C. Optimum divacancy resonance signals were observed after an electron fluence of about 1.5×10^{18} electrons/cm^2 for both kinds of samples.

In addition to the EPR spectrum $G7$ of the negative divacancy, in both kinds of samples different series of EPR spectra from other defects have been observed.[31,32] In the originally high-resistivity samples spectrum $G7$ could not be observed without simultaneous perceptibility of spectrum $G16$. In the low-resistivity samples spectrum $G7$ always appeared together with spectrum $NL7$.[31]

The magnetic resonance experiments were carried out in a superheterodyne spectrometer operating at 23 GHz.[33,34] Experiments were performed for the greater part as described in I. Samples were mounted with their axis along the axis of a cylindrical TE_{011} cavity. The ENDOR coil consisted of two vertical oblong rectangular loops of fine copper wire fixed to a Teflon cylinder which could be shifted over the sample. During ENDOR measurements the sample temperature was kept at about 10 K. At this temperature the spin-lattice relaxation time T_1 of the divacancy is in the 0.01–0.1s region.[35] For our conditions the EPR signal is saturated at that temperature. For double phase-sensitive detection the magnetic field was modulated sinusoidally at a frequency of 127 Hz, while the square-wave modulation of the rf field had a frequency of about 1.4 Hz. The ENDOR spectra of the smaller hyperfine interactions were recorded with the magnetic field adjusted to the center of an EPR line. For the larger interactions the magnetic field setting was changed, approximately to the expected or observed position of the corresponding hyperfine satellite of the EPR transition.

On samples of both kinds described above, hyperfine interactions have been observed with ENDOR. For the lower-frequency interactions no differences could be observed although the low-resistivity samples showed greater EPR intensities. For the larger interactions the results on the low-resistivity samples got even worse by severe line broadening. Therefore the higher-frequency interactions have all been determined on the high-resistivity material.

III. DESCRIPTION AND ANALYSIS OF ENDOR SPECTRA

A. Spin Hamiltonian

EPR and ENDOR spectra of a paramagnetic defect in silicon in which no impurity atoms are involved can generally be described by the spin Hamiltonian

$$\mathcal{H} = \mu_B \vec{H}\cdot\vec{\vec{g}}\cdot\vec{S} + \sum_i (\vec{S}\cdot\vec{\vec{A}}_i\cdot\vec{I}_i - g_N\mu_N\vec{H}\cdot\vec{I}_i) \qquad (1)$$

with an electronic Zeeman interaction term, a hyperfine interaction term, and a nuclear Zeeman interaction term in which the parameter i enumerates the lattice sites around the defect. For each lattice site there is a 4.7% probability to be occupied by a ^{29}Si isotope with a nuclear spin $I=\frac{1}{2}$ and a nuclear g value $g_N=-1.1095$.

The EPR spectrum $G7$ of the negative divacancy can be described with an electron spin $S=\frac{1}{2}$ and an anisotropic electronic Zeeman interaction. The components of the electronic g tensor are found to be

$$g_{xx}=2.01165\pm0.0001,$$
$$g_{yy}=g_{zz}=2.00895,$$
$$g_{xy}=g_{xz}=-0.0042,$$
$$g_{yz}=-0.00445,$$

for a divacancy in the orientation labeled *ad* and the coordinate system as given in Fig. 1. These values agree with those reported by Watkins and Corbett.[5]

In the limit of high magnetic field a solution of the eigenvalue problem of the spin Hamiltonian

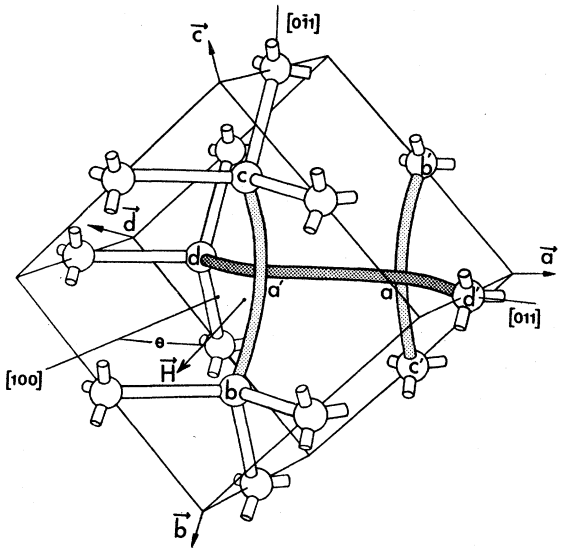

FIG. 1. Model of the divacancy in the orientation ad. The empty lattice sites are a and a'.

Eq. (1) can easily be found. In that case ENDOR transition frequencies submitted to the selection rules $\Delta m_s = 0, \Delta m_{I_i} = 1, \Delta m_{I_{j\neq i}} = 0$ are given by

$$h\nu_i^{\pm} = |g_N\mu_N H \pm \tfrac{1}{2}\hat{h}\cdot\vec{\mathbf{A}}_i\cdot\hat{h}| , \tag{2}$$

where $\hat{h}$ is a unit vector in the direction of the external magnetic field $\vec{\mathbf{H}}$. In this way the resonances from different neighboring nuclei give rise to a spectrum which is symmetric with respect to the nuclear Zeeman frequency $h\nu = g_N\mu_N H$. An illustration is given in Fig. 2. Another striking feature of this spectrum is the large signal directly around the nuclear Zeeman frequency, which originates from nuclear transitions of large numbers of neighbors with very weak unresolved interactions. In the low-resistivity samples with a high phosphorus content (about 1 upon 70 000) an additional resonance was observed around the nuclear Zeeman frequency of the ^{31}P nucleus ($g_N = 2.261$). This is an indication that there are still hyperfine interactions with very distant neighbors.

The high-field solution Eq. (2) breaks down if the anisotropic part of the hyperfine tensor $\vec{\mathbf{A}}_i$ is no longer small as compared to the transition frequency $h\nu^{\pm}$, as for most larger interactions. For such cases a corrected formula

$$(h\nu^{\pm})^2 = (g_N\mu_N H \pm \tfrac{1}{2}\hat{h}\cdot\vec{\mathbf{A}}_i\cdot\hat{h})^2 + \tfrac{1}{4}[(\hat{h}\cdot\vec{\mathbf{A}}_i)\times\hat{h}][(\hat{h}\cdot\vec{\mathbf{A}}_i)\times\hat{h}] \tag{3}$$

can be derived.

For an analysis of hyperfine interactions it is appropriate to separate the tensors $\vec{\mathbf{A}}_i$ into a scalar part a_i and a traceless tensor $\vec{\mathbf{B}}_i$

$$\vec{\mathbf{A}}_i = a_i\vec{\mathbf{I}} + \vec{\mathbf{B}}_i \tag{4}$$

with $a_i = \frac{1}{3}\mathrm{Tr}\vec{\mathbf{A}}_i$ and $\mathrm{Tr}\vec{\mathbf{B}}_i = 0$. The isotropic part a_i originates from the Fermi contact interaction

$$a_i = \tfrac{8}{3}\pi g\mu_B g_N\mu_N|\psi(\vec{\mathbf{r}}_i)|^2 \tag{5}$$

giving a relation with the probability density of the defect electron on the nuclear site $\vec{\mathbf{r}}_i$. The anisotropic part of the interaction arises from the dipole-dipole coupling between the electronic and nuclear magnetic moments

$$(B_i)_{jk} = g\mu_B g_N\mu_N\langle\psi|3r_j r_k/r^5 - \delta_{jk}/r^3|\psi\rangle , \quad j,k = x,y,z . \tag{6}$$

B. Symmetry considerations

In Fig. 1 the x,y,z crystal coordinate system is given which is used in this paper. The divacancy orientation depicted, with vacant lattice sites on a' and a and dangling or extended bonds on d and d' is denoted by ad, according to Watkins and Corbett.[5] In our analysis the orientation ad is chosen as the basic orientation for which the hyperfine interaction tensors are given. A group-theoretical treatment of the divacancy with its shells of neighboring lattice sites has been given in I. In an undistorted lattice a divacancy will have $\bar{3}m$ (D_{3d}) point-group symmetry. As a result of Jahn-Teller instability a lattice distortion gives the lower $(2/m)(C_{2h})$ symmetry. The presence of a neighboring ^{29}Si nucleus further lowers the symmetry. If the nucleus is present on the mirror plane of the divacancy the point-group symmetry is reduced to $m(C_{1h})$. Two such lattice sites about a divacancy of a given orientation which are equivalent by symmetry are said to form a shell. All shells of this type constitute the mirror-plane class. The atom sites d and d' in Fig. 1 are an example of a mirror-plane calss shell. A ^{29}Si nucleus which is not situated in the mirror plane of the divacancy lowers the symmetry to point group 1 (C_1). These lattice sites divide in shells which are called general class shells. Each shell contains four lattice sites equivalent by symmetry. Each lattice site about a divacancy belongs to a shell of one of these two classes. In magnetic resonance practice of silicon the external magnetic field is generally rotated in a {110} plane of a crystal. In that way the different divacancy orientations which are present, combined with the possible positions of a ^{29}Si nucleus in a shell, give rise to characteristic angular-dependent patterns. Mirror-plane class hyperfine interactions exhibit patterns of monoclinic I symmetry, general class interactions of triclinic symmetry.[34] In Figs. 3

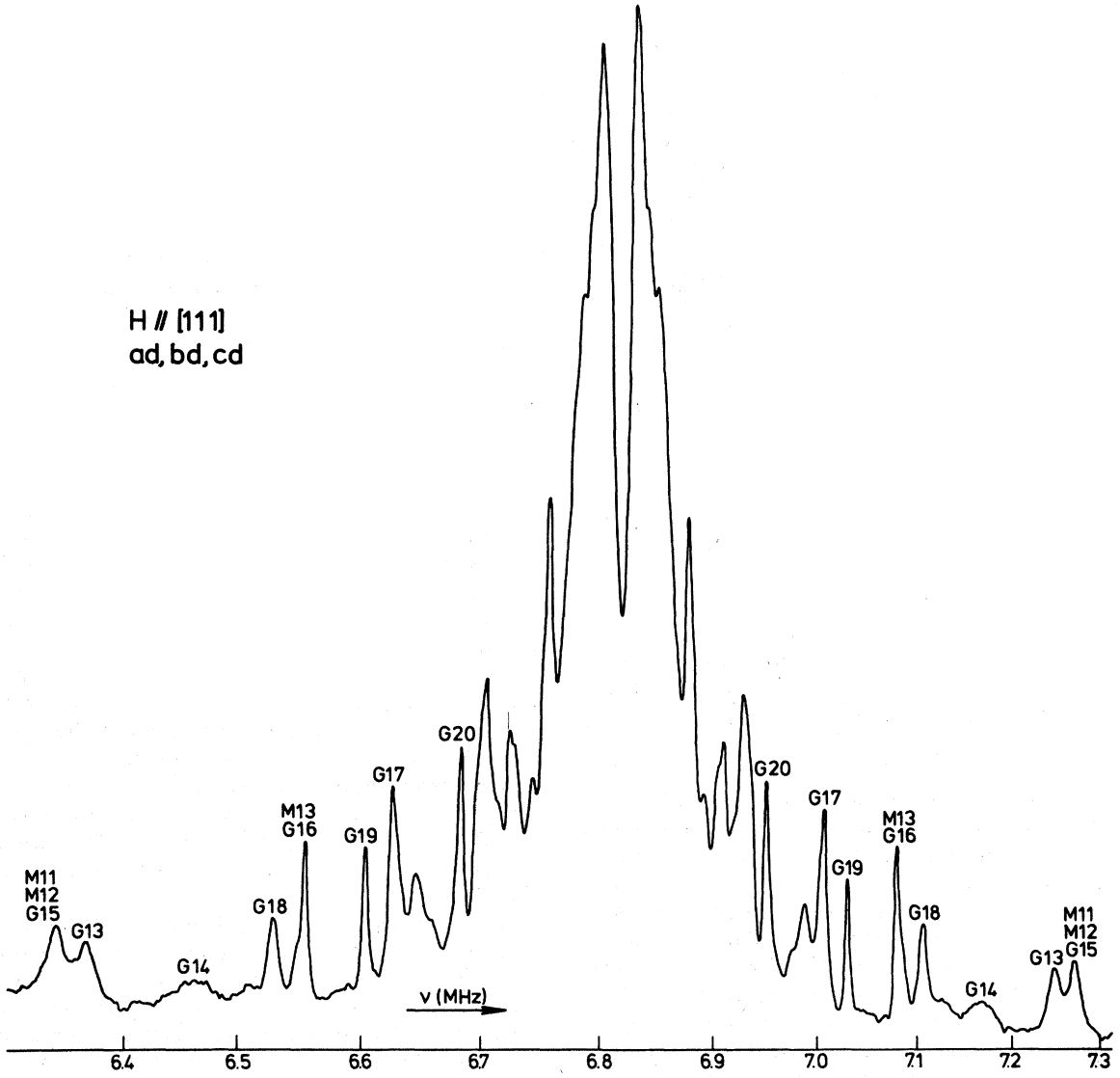

FIG. 2. Central part of an ENDOR spectrum for the divancancy orientations *ad*, *bd*, and *cd*, with $\vec{H} \| [111]$. The spectrum shows symmetry around the central frequency $\nu = 6.818$ MHz.

and 4 such patterns are shown. For magnetic field directions in the ⟨100⟩, ⟨111⟩, and ⟨011⟩ directions characteristic degeneracies occur. The values of the hyperfine interactions in these directions are labeled S_i, T_i, and U_i, respectively.

C. Determination of hyperfine tensors

To produce the angular-dependent patterns indicated above, the hyperfine interaction has to be determined for a variety of magnetic field directions in the $(01\bar{1})$ plane and for all different divacancy orientations. On the other hand a general class tensor is determined by only six independent tensor elements and a mirror-plane class tensor by only four. Therefore a determination of the S, T, and U values from each tensor is far sufficient to determine the tensors. The symmetry type of a tensor follows directly from the number of S, T and U values. Since in each of the S, T, and U values transitions coincide which are related to different defect orientations, these resonances can be determined with a better signal-to-noise ratio than those for an arbitrary direction of the magnetic field. The tensor elements can be derived with a least-squares fit to these observed values. Examples of the patterns, calculated from tensors which have been derived in this way are given in Figs. 3 and 4 for a mirror-plane class and a general class inter-

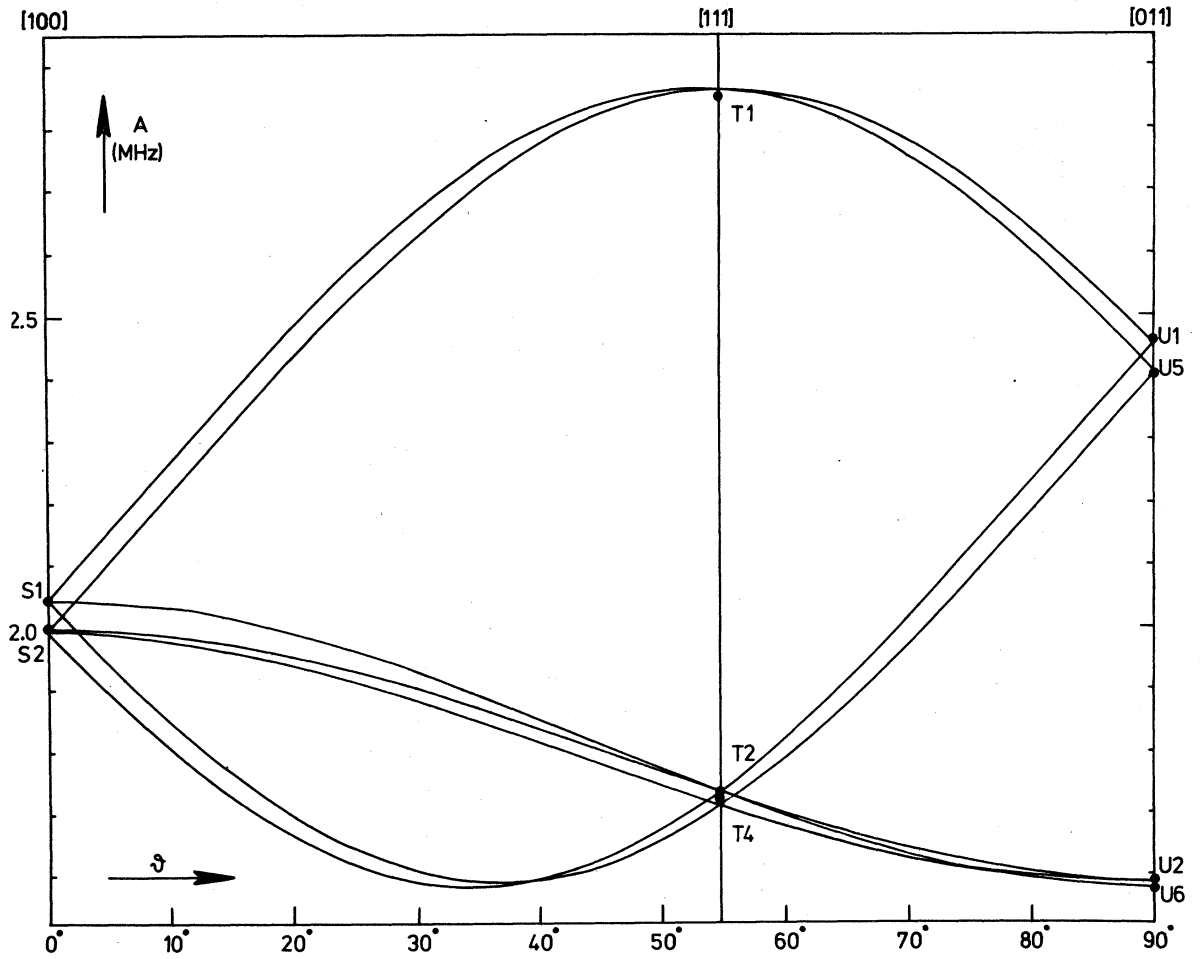

FIG. 3. Angular dependence of the mirror-plane class hyperfine interaction $M5$. Least-squares fit to the observed S, T, and U values which are given as black dots. This interaction has nearly ⟨111⟩ axial symmetry.

action, respectively. In the frequency range where most of the hyperfine interactions were found, the angular-dependent patterns showed such a severe overlap that in most cases it was absolutely impossible to decide which S, T, and U values would belong to the same shell. For this reason spectra were recorded for magnetic field directions at 5° intervals and with the field set upon the EPR transitions which correspond to each of the orientations ad, da, and bc, cb. In regions of crossing lines even 2° or 1° intervals have been taken. On the other hand some angles of the magnetic field had to be omitted due to overlap of the EPR resonances with those of other orientations or those of other defect spectra. An angular plot of the observed hyperfine frequencies is given in Fig. 5 for a large part of the considered frequency range. For a mirror-plane class tensor the tensor elements can be derived from the observed S, T, and U values of the four divacancy orientations as given in Fig. 5. The other S and U values may be calculated and afterwards experimentally verified. Predicted values turned out to be accurate to within a few kHz. A general class tensor cannot yet be determined unambiguously in this way. From the calculated sum $S_2 + S_3$ of the S values from other divacancy orientations and a list of experimentally determined values S_2 and S_3, in all cases a decisive choice could be made, however. The other values could again be calculated and afterwards experimentally verified. Tensor components derived by a least squares fit of $\hat{h} \cdot \bar{\bar{A}} \cdot \hat{h}$ to the observed S, T, and U values served as starting parameters for a numerical diagonalization of the complete spin Hamiltonian Eq. (1). Iterative calculations produced a final least-squares fit of the tensor components.

The general class tensors have been labeled Gi, the mirror-plane class tensors Mi, enumerating them after decreasing isotropic part as in I.

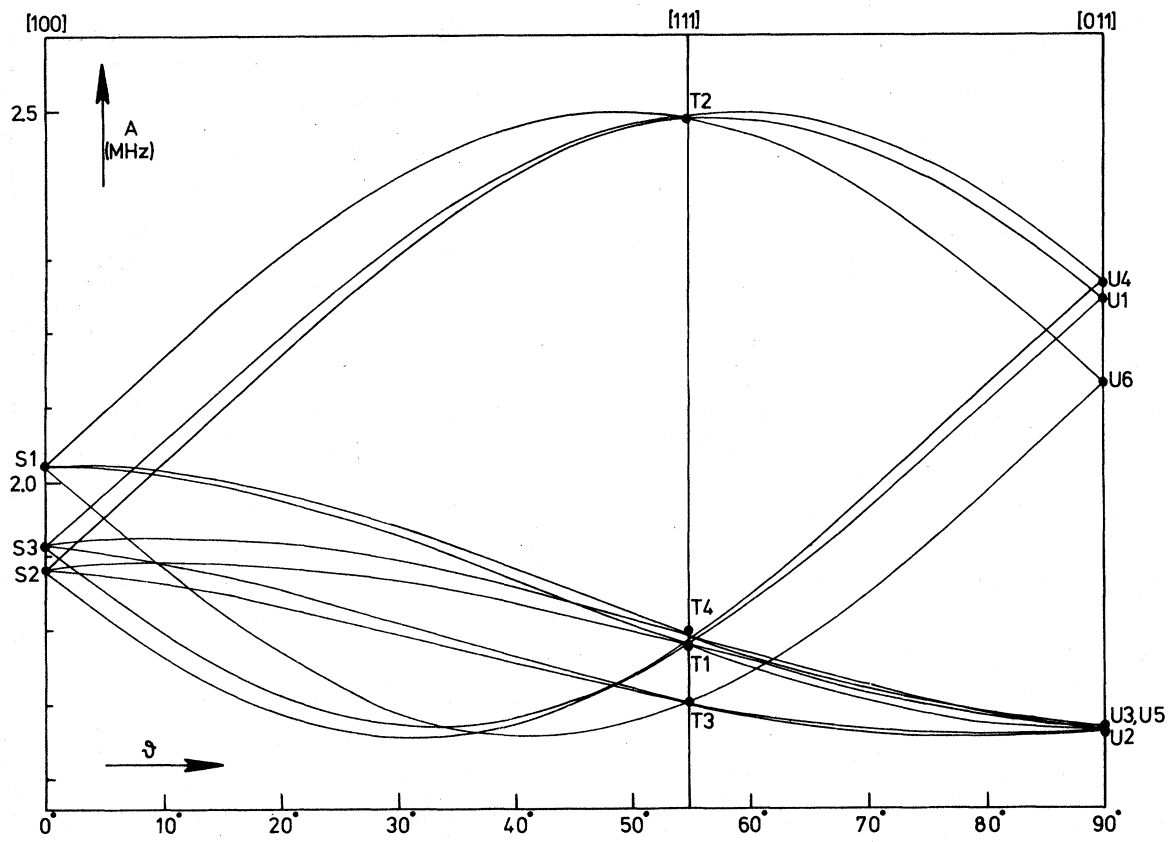

FIG. 4. Angular dependence of the nearly ⟨111⟩ axially symmetric general class tensor $G8$.

A total of 20 general class tensors has been determined. From the 13 mirror-plane class tensors one ($M1$) has been observed only with EPR. In Table I the hyperfine parameters of these 33 interactions are given. The tensor components specified in the crystal coordinate system are given for divacancy orientation *ad*. For a mirror-plane class shell the interactions with both lattice sites of the shell are given by this tensor. For the four lattice sites of a general class shell there are two tensors which transform into each other by interchange of the y and z indices. From experiment it is not possible to determine to which two lattice sites the given tensors correspond. The three principal values of the tensors are called A_1, A_2, and A_3 in order of descending magnitudes. The directions of their principal axes are specified by the angles γ_i and δ_i, where γ_i is the angle between the ith eigenvector and the $(0\bar{1}1)$ mirror plane of the divacancy and δ_i is the angle from the [100] direction to the projection in the $(0\bar{1}1)$ plane. For a mirror-plane class tensor one principal axis always points into the $[0\bar{1}1]$ direction. The reported hyperfine interactions cover 106 lattice sites around the divacancy. Hyperfine interactions with at least 10 additional shells were observed, resolved from the central part of the ENDOR spectrum around the nuclear Zeeman frequency. The overlap of the angular-dependent patterns of these weaker interactions was too strong to determine their hyperfine tensors. The tensor components for the smallest interactions could be determined to ±1 kHz, typical linewidths were 3–5 kHz. For larger interactions both error limit and linewidth increased. For $G1$, $G2$, and $M2$ tensor components are accurate to ±20 kHz; linewidths became even 100 kHz. EPR results of $M1$ are accurate to within 0.5 MHz and agree with results reported before.[5]

IV. DISCUSSION

A. Analysis in atomic orbitals

For the analysis of hyperfine interactions it has turned out to be appropriate to describe a defect wave function as a molecular orbital which is constructed by linear combination of atomic orbitals.[5,36,37] In this case a linear combination of silicon $3s$ and $3p$ atomic orbitals centered on the lattice sites around the divacancy can be chosen:

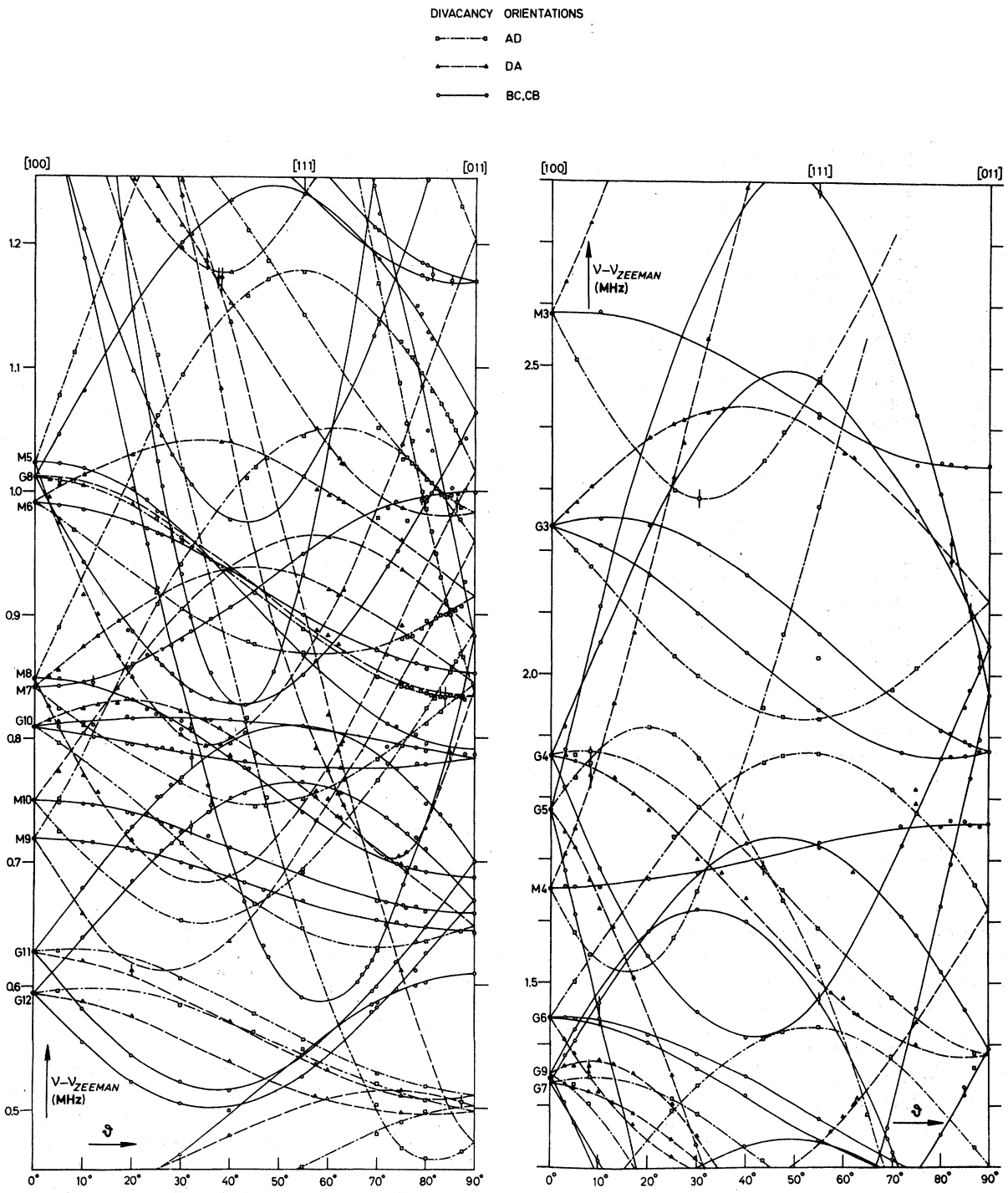

FIG. 5. Angular-dependent plot of the observed hyperfine frequencies from the divacancy orientations *ad*, *da*, and *bc*, *cb*. The frequency ranges from 0.5 to 2.8 MHz above the nuclear Zeeman frequency.

TABLE I. Hyperfine parameters of the negative divacancy (values in MHz, γ_1, δ_1, γ_2 in degrees).

Tensor	A_{xx}	A_{yy}	A_{zz}	A_{xy}	A_{yz}	A_{zx}	A_1	A_2	A_3	γ_1	δ_1	γ_2
$G1$	31.59	32.26	30.56	2.21	−2.28	−2.09	35.93	29.70	28.78	−54.4	10.7	25.3
$G2$	20.13	19.85	19.85	3.16	3.10	3.24	26.28	16.83	16.73	0.2	53.6	30.8
$G3$	4.480	3.888	4.111	−0.258	0.243	−0.437	4.891	3.856	3.731	− 8.4	−38.2	4.2
$G4$	3.704	3.211	3.621	−0.688	−0.652	0.804	4.976	2.857	2.703	49.8	8.4	−30.8
$G5$	3.441	1.549	3.838	−0.931	−1.099	1.845	5.964	1.786	1.077	46.1	24.0	−29.9
$G6$	2.876	2.858	2.711	0.506	0.446	0.447	3.755	2.362	2.329	− 3.4	52.4	23.5
$G7$	2.660	2.499	2.243	0.595	−0.399	−0.478	3.490	1.982	1.929	−46.9	8.3	24.3
$G8$	2.016	1.882	1.909	0.287	−0.229	−0.294	2.485	1.668	1.654	−48.7	− 1.5	14.4
$G9$	2.668	1.173	1.509	0.464	−0.400	−0.832	3.272	1.177	0.900	−31.3	− 8.9	58.2
$G10$	1.616	1.477	1.395	−0.110	−0.137	−0.065	1.677	1.557	1.253	23.0	−20.6	−66.4
$G11$	1.252	1.166	1.251	−0.191	−0.192	0.213	1.624	1.038	1.006	52.2	6.7	−30.8
$G12$	1.188	1.120	1.217	−0.156	−0.170	0.203	1.535	0.999	0.991	52.8	10.4	−33.0
$G13$	0.784	0.692	0.772	0.130	−0.017	0.051	0.885	0.773	0.590	− 9.4	35.2	−65.4
$G14$	0.724	0.722	0.722	−0.024	−0.011	−0.003	0.748	0.725	0.695	40.6	−28.0	−46.1
$G15$	0.724	0.667	0.720	0.094	0.093	0.116	0.910	0.606	0.595	5.6	51.0	−27.1
$G16$	0.572	0.606	0.562	−0.105	0.105	−0.084	0.778	0.485	0.476	5.0	−56.8	0.2
$G17$	0.420	0.448	0.408	−0.056	−0.049	0.039	0.525	0.376	0.374	55.5	−16.4	−15.6
$G18$	0.420	0.388	0.427	0.076	0.076	0.098	0.581	0.329	0.325	5.7	52.3	−83.0
$G19$	0.388	0.428	0.405	−0.043	0.050	0.024	0.473	0.419	0.329	12.6	−73.9	35.7
$G20$	0.319	0.287	0.284	−0.064	−0.045	0.063	0.415	0.241	0.235	46.8	− 0.7	− 5.2
$M1$	197.4	$=A_{zz}$	194.1	$=A_{zx}$	22.3	23.7	241.7	172.0	171.8	0	53	90
$M2$	11.21		11.49		2.07	1.93	15.36	9.42	9.42	0	56.6	90
$M3$	5.151		5.440		0.768	−0.693	6.794	4.672	4.565	0	−59.2	90
$M4$	3.270		4.988		1.486	−0.676	6.738	3.502	3.007	0	−74.6	90
$M5$	2.038		1.989		0.413	0.430	2.855	1.585	1.576	0	53.3	0
$M6$	1.978		1.770		0.062	−0.108	2.074	1.736	1.709	0	−32.1	0
$M7$	1.681		1.847		−0.160	−0.136	2.007	1.877	1.492	90	(a)	0
$M8$	1.693		1.704		0.333	0.326	2.358	1.373	1.371	0	55.2	0
$M9$	1.430		1.602		0.317	0.254	2.109	1.286	1.239	0	62.1	90
$M10$	1.495		1.530		0.209	−0.205	1.932	1.320	1.303	0	−56.4	90
$M11$	0.823		1.118		−0.102	−0.039	1.219	1.031	0.808	90	(b)	0
$M12$	0.720		0.691		0.089	0.101	0.895	0.605	0.602	0	50.9	0
$M13$	0.386		0.551		−0.060	0.057	0.611	0.534	0.343	90	(c)	0

(a) $\delta_2 = -45.5$ (b) $\delta_2 = -75.2$ (c) $\delta_2 = 61.7$

$$\psi = \sum_i \eta_i (\alpha_i \psi_{3s} + \beta_i \psi_{3p}) . \tag{7}$$

Such a wave function gives rise to axially symmetric hyperfine interactions if only the atomic orbitals centered on the relevent nuclear site are considered. In that case the Fermi-contact interaction Eq. (5) reduces to

$$a_i = \tfrac{8}{3}\pi g \mu_B g_N \mu_N \eta_i^2 \alpha_i^2 |\psi_{3s}(0)|^2 . \tag{8}$$

The dipole-dipole part of the interaction Eq. (6) in diagonal form reduces to

$$\vec{\vec{B}}_i = \begin{pmatrix} 2b_i & 0 & 0 \\ 0 & -b_i & 0 \\ 0 & 0 & -b_i \end{pmatrix} \tag{9}$$

with

$$b_i = \tfrac{2}{5} g \mu_B g_N \mu_N \eta_i^2 \beta_i^2 \langle 1/r^3 \rangle_{3p} . \tag{10}$$

For the analysis of the present data the tensors were transformed to diagonal form and reduced to

$$\vec{\vec{A}} = \begin{pmatrix} A_1 & 0 & 0 \\ 0 & A_2 & 0 \\ 0 & 0 & A_3 \end{pmatrix} \equiv \begin{pmatrix} a+2b & 0 & 0 \\ 0 & -b+c & 0 \\ 0 & 0 & a-b-c \end{pmatrix} . \tag{11}$$

in which c gives the deviation from axial symmetry. The values a, b, and c are shown in Table II. From the 20 general class interactions 16 are approximately axially symmetric around the $\vec{A}_1$ eigenvector. From the 13 mirror-plane class interactions 10 tensors show this property. Moreover 21 of these 26 axially symmetric interactions have their axial direction near one of the ⟨111⟩ crystal bond directions. These axial directions are also given in Table II, denoted by a, b, c, and d according to Fig. 1. The fraction of ⟨111⟩ axial-

TABLE II. Reduced hyperfine parameters (MHz), axial direction, and derived LCAO parameters.

Tensor	a	b	c	Axis	α^2	β^2	η^2 (%)
$G1$	31.47	2.23	0.46	b/c	0.256	0.744	2.97
$G2$	19.94	3.17	0.05	d	0.133	0.867	3.61
$G3$	4.159	0.386	0.063		0.218	0.782	0.46
$G4$	3.512	0.732	0.077	b/c	0.105	0.895	0.81
$G5$	2.942	1.511	0.355		0.045	0.955	1.56
$G6$	2.815	0.470	0.017	d	0.128	0.872	0.53
$G7$	2.467	0.512	0.027	b/c	0.105	0.895	0.57
$G8$	1.936	0.275	0.007	b/c	0.147	0.853	0.32
$G9$	1.783	0.745	0.139	$\perp b/c$	0.055	0.945	0.78
$G10$	1.496	0.091	0.152	no	0.287	0.713	0.13
$G11$	1.223	0.201	0.016	b/c	0.130	0.870	0.23
$G12$	1.175	0.180	0.004	b/c	0.138	0.862	0.21
$G13$	0.750	0.068	0.092	no	0.213	0.787	0.09
$G14$	0.723	0.013	0.015	no	0.582	0.418	0.03
$G15$	0.704	0.103	0.006	d	0.143	0.857	0.12
$G16$	0.580	0.099	0.005	a	0.125	0.875	0.11
$G17$	0.425	0.050	0.001	b/c	0.172	0.828	0.06
$G18$	0.412	0.085	0.002	d	0.106	0.894	0.09
$G19$	0.407	0.033	0.045	no	0.232	0.768	0.04
$G20$	0.297	0.059	0.003	b/c	0.110	0.890	0.07
$M1$	195.2	23.3	0.1	d	0.170	0.830	27.71
$M2$	11.40	1.98	0.00	d	0.123	0.877	2.23
$M3$	5.344	0.725	0.054	a	0.153	0.847	0.85
$M4$	4.416	1.161	0.248		0.085	0.915	1.25
$M5$	2.005	0.425	0.005	d	0.103	0.897	0.47
$M6$	1.840	0.117	0.014	$\perp d$	0.277	0.723	0.16
$M7$	1.792	0.107	0.193	no	0.290	0.710	0.15
$M8$	1.701	0.329	0.001	d	0.112	0.888	0.37
$M9$	1.545	0.282	0.024	d	0.118	0.882	0.32
$M10$	1.518	0.207	0.009	a	0.152	0.848	0.24
$M11$	1.019	0.100	0.112	no	0.200	0.800	0.12
$M12$	0.701	0.097	0.002	d	0.150	0.850	0.11
$M13$	0.496	0.058	0.096	no	0.174	0.826	0.07

ly symmetric interactions is about the same as for the positive divacancy as given in I. For the constants of the atomic silicon wave function appearing in Eqs. (8) and (10) values given by Watkins and Corbett[36] can be taken: $|\psi_{3s}(0)|^2 = 31.5 \times 10^{24}$ cm^{-3} and $\langle 1/r^3\rangle_{3p} = 16.1 \times 10^{24}$ cm^{-3}. Substituting these values and using $\alpha^2 + \beta^2 = 1$ one derives from each hyperfine interaction the localization (η^2) and the s and p character (α^2 and β^2, respectively) of the defect electron on the lattice sites of the corresponding shell. These values are also given in Table II, exhibiting a slightly less localized wave function than the positive charge state.[37] For an electron in an orbital pointing in any of the four $\langle 111\rangle$ bond directions in the silicon lattice, a sp^3 hybridized orbital might be expected. Inspection of Table II shows that the $\langle 111\rangle$ axially symmetric tensors generally show a deviation from $\alpha^2 = 0.25$. On the average only 16.5% s character is found. For a proper set of basis functions the values η_i^2 should add up to 100%. The too large value $\Sigma\eta_i^2 = 119\%$ is probably due to the nonorthogonality of the atomic orbitals which are centered on different lattice sites and to the nonaxial interactions for which the values η_i^2 have little significance.

The origins of the deviations from axial symmetry and the strong p character of the wave function as it is reflected in the hyperfine interactions require a further examination. Especially for the dipole-dipole term as reduced to Eqs. (9) and (10) corrections have to be included. Unpaired charge densities on neighboring lattice sites and overlap between atomic orbitals can contribute to considerable deviations both from the axial direction as from the axial character itself.[33] The latter can also be brought about by including $3d$ orbitals in the LCAO treatment. It is not quite possible, however, to elaborate such corrections for all lattice sites, certainly not as a matching between

tensors and definite shells of lattice sites is not yet possible.

B. Results from extended Hückel theory calculations

For a theoretical calculation of wave functions and energy levels of deep level defects in a covalent solid as silicon semiempirical EHT calculations have been shown to be rather successful.[26] The theory works best for systems where the differences in electronegativity are not too great. As intrinsic point defects in elemental covalent semiconductors are probably in this category, EHT has been applied to these systems in a number of cases.[38,39] As the detailed information from ENDOR experiments yields a severe test for a theory like this, it is important to compare between theory and experiment, both to describe the experiment and to examine the reliability of the theoretical method.

EHT uses molecular orbitals ψ_i which are linear combinations of atomic orbitals ϕ_j

$$\psi_i = \sum_k c_{ki}\phi_k \,. \tag{12}$$

For the atomic orbitals generally Slater-type $3s$ and $3p$ orbitals are chosen. A solution for the secular equations

$$\sum_k (H_{jk} - \epsilon_i S_{jk}) c_{ki} = 0 \tag{13}$$

yields the wave-function coefficients c_{ki} and the energy eigenvalues ϵ_i. A solution is obtained using the Wolfsberg-Helmholtz approximations

$$H_{jk} = \langle \phi_j | \mathcal{H} | \phi_k \rangle = -\tfrac{1}{2} K_{jk}(I_j + I_k) S_{jk} \,, \quad j \neq k \tag{14}$$

and

$$H_{jj} = -I_j \tag{15}$$

in which $S_{jk} = \langle \phi_j | \phi_k \rangle$, I_j is the empirical ionization energy of orbital j, and K_{jk} is a parameter between 1 and 2. The parameter K_{jk} will generally be adjusted empirically, for instance, to reproduce the known silicon band structure in a calculation for the perfect lattice.

Defect calculations can be performed for a finite cluster with a defect in its center or for an infinite lattice constituted by a periodic repetition of clusters with such a shape that no empty sites

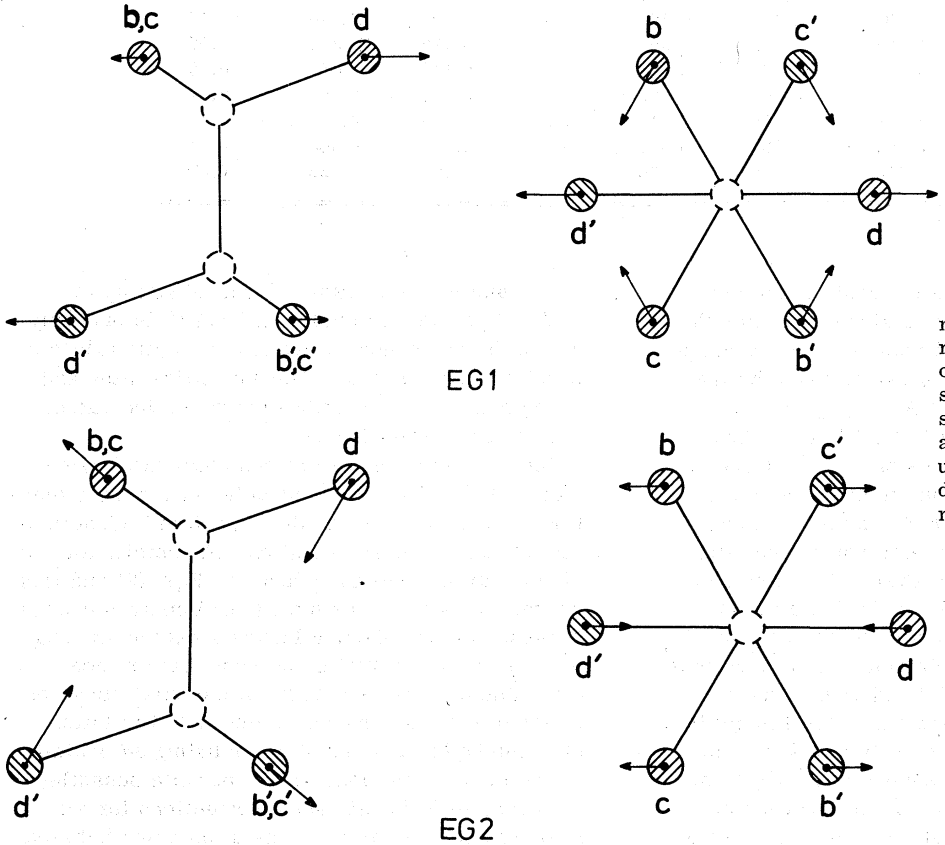

FIG. 6. Two main symmetry-lowering distortion modes (a) $EG1$ and (b) $EG2$ of the divacancy with its six nearest neighbors in sideview and topview. The arrows correspond to one unit of distortion, which is defined as an rms displacement of the six atoms of 1 Å.

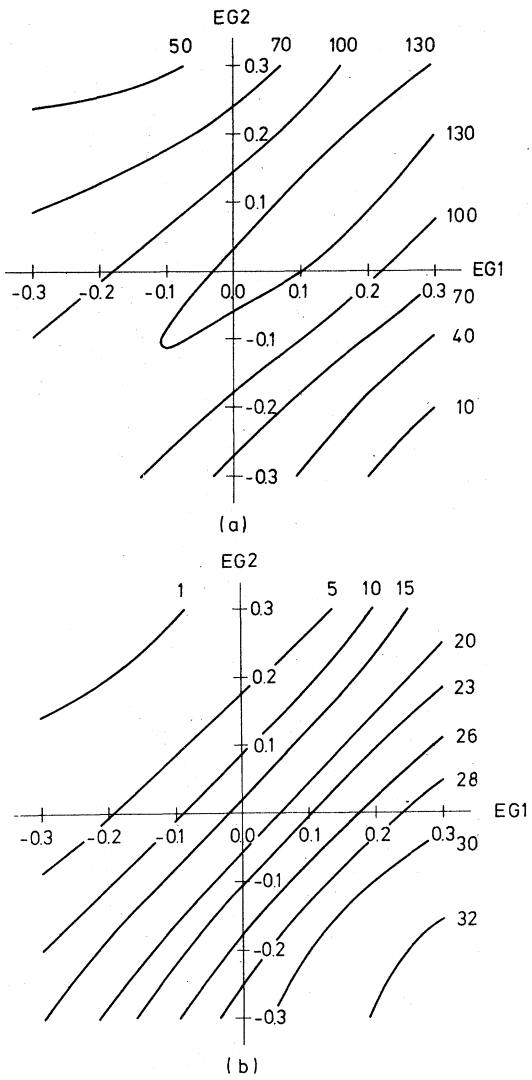

FIG. 7. (a) Isotropic part a, (b) axial part b of the hyperfine interaction tensor for the shell of atoms d and d' as function of the distortion parameters $EG1$ and $EG2$. Calculation for a wave function of symmetry b_u.

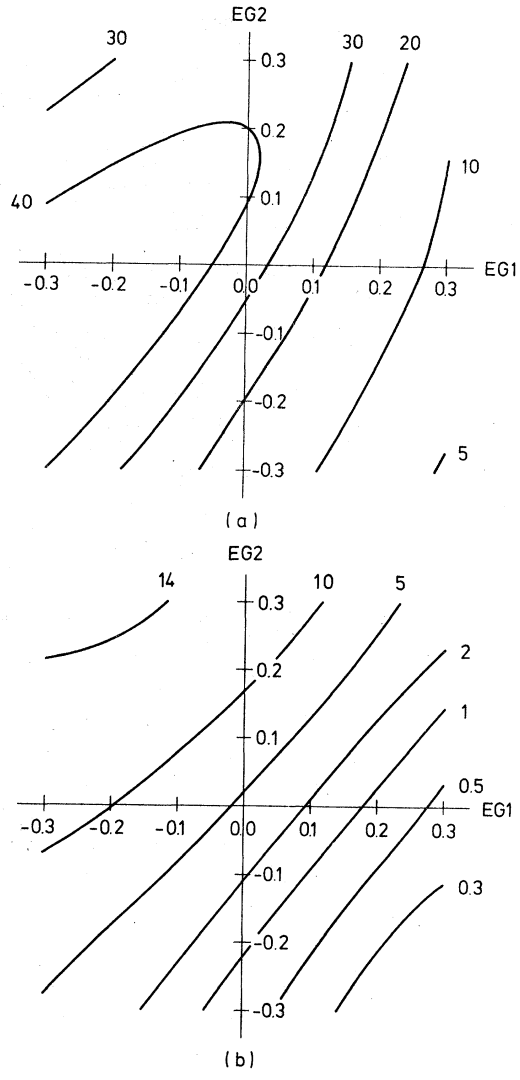

FIG. 8. Same data as in Fig. 7 calculated for the shell of atoms b, c, b', and c'.

are left between. With this molecular unit cell approach (MUCA) the disturbing effect of unpaired surface states of an isolated cluster and the extra charges required to satisfy these bonds can be removed.

With MUCA, calculations for the divacancy in a 64-atom cluster had been performed already by Lee and McGill.[27] With application of a Jahn-Teller distortion they find two defect levels in the band gap, one of symmetry b_u below one of symmetry a_g. These are the right symmetries but in reversed order as compared to those derived in a simpler treatment by Watkins and Corbett.[5] MUCA calculations have also been performed especially to describe hyperfine interactions using slightly different orbitals and EHT parameters.[28,29] From these calculations it is also argued that in the positive charge state of the divacancy the unpaired electron occupies a level of symmetry b_u. For this level a systematical study of the effect of different Jahn-Teller distortion modes has been made in order to obtain a best fit with experimental results from I. It turned out that there was a promising region of values for both main distortion modes, for which satisfactory agreement could be obtained between observed hyperfine interactions and theoretical values for two shells of nearest neighbors of the divacancy.[29] In Fig. 6 the

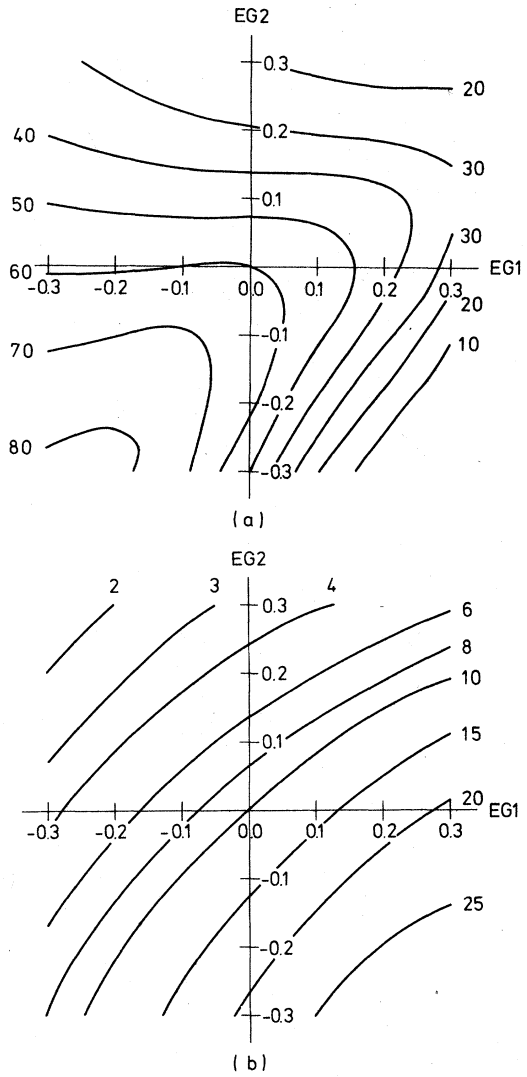

FIG. 9. (a) Isotropic part a, (b) axial part b of the hyperfine interaction tensor for the shell of atoms d and d' calculated for a wave function of symmetry a_g.

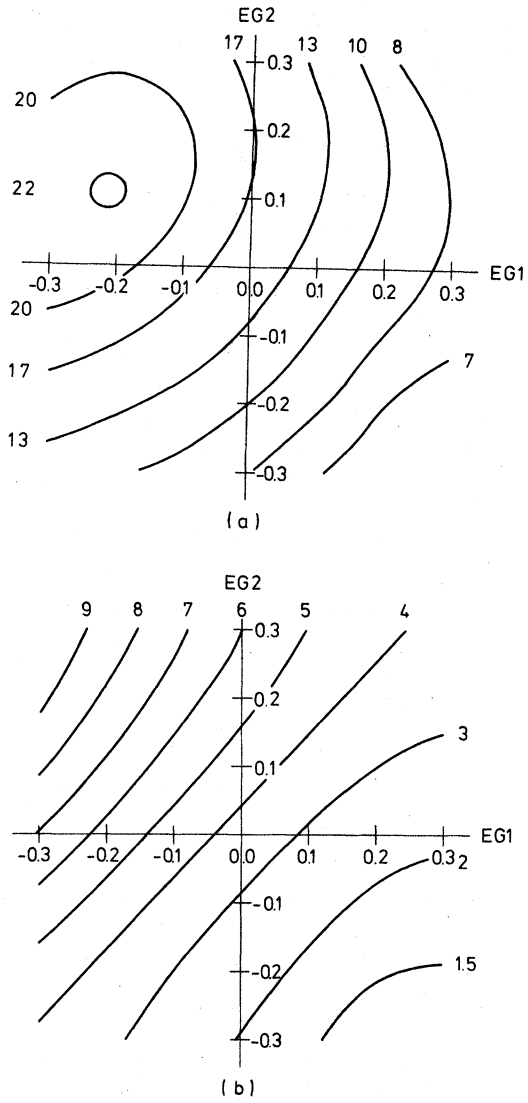

FIG. 10. Same data as in Fig. 9 calculated for the shell of atoms b, c, b', and c'.

two main distortion modes are represented. The hyperfine parameters a and b were calculated as a function of these two distortions. In that way for V_2^+ the largest mirror-plane interaction $M1$ could be ascribed to the shell of lattice sites d and d' in Fig. 1, as should also be expected from simple considerations. For the nearest-neighbor general class shell (atom sites b, c, b', and c' in Fig. 1) from theory a better agreement with tensor $G1$ than with $G2$ had been obtained. This was in contradiction, however, with earlier conclusions from motionally averaged EPR spectra.[1,5] The significance of the experimental assignment of this shell to $G2$ rather than to $G1$ or $G3$, however, is less than suggested in I, as would follow from a similar uncertainty in the averaged hyperfine interactions as presently found for V_2^- (Sec. IV C). In Figs. 7 and 8 the calculated results are given. A simultaneous accurate fit of $M1$ and $G1$ or $G2$ of V_2^+ could not be obtained. There is, however, some agreement for distortion values of $0.05 < EG1 < 0.1$ and $-0.05 < EG2 < 0.03$.

To obtain the negative charge state of the divacancy the next higher energy level has to be considered whose wave function has a large localization on the divacancy. The only one in the band gap which deserves consideration turns out to have a_g symmetry. For this level and wave

function, ascribed to the negative charge state, hyperfine parameters have also been calculated for the nearest-neighbor mirror-plane class and general class shells. In Figs. 9 and 10 values for a and b for the two nearest-neighbor shells are given as a function of the two main distortion modes of Fig. 6. A comparison with the experimental results of Table II shows large discrepancies in most cases. It is evident that a simultaneous fit for both parameters and both shells of V_2^- is not even approximately possible.

From the simple considerations of Watkins and Corbett[5] it followed that the unpaired electron of V_2^+ occupied a level of symmetry a_g and that of V_2^- a level of symmetry b_u. This reversed order as compared to the EHT results seemed reasonable as the a_g level corresponds mainly to an extended bondinglike orbital between both mirror-plane class nearest neighbors, while the b_u level arose from such an antibondinglike orbital whose energy is generally higher. A closer examination of the energy levels near the bandgap which result from the present EHT calculations reveals some problems as already indicated earlier.[28,29] Not all levels in the bandgap show a high localization on the divacancy and not all localized levels are in the bandgap. Likewise the filling of calculated levels is not performed consistently in order of increasing energy in all cases. Moreover the order of resulting levels also depends on the magnitude of the distortion and on the point of k space for which calculations have been performed. This all may be indications that the detailed positions of energy levels relative to each other, as resulting from EHT calculations, are not very significant. Therefore it is equally possible that the energy levels have to be filled in such an order that the levels of symmetry a_g and b_u have to be assigned to the charge states of the divacancy in the way Watkins and Corbett did. To explore this equally probable possibility, EHT results have to be compared with experimental values in that way. To facilitate such a comparison, values of the hyperfine parameters a and b are given in Table III for the four largest interactions for both V_2^+ and V_2^-.

If V_2^- is identified with the b_u level, the theoretical values for the hyperfine parameters of the shell of atoms d and d' are too low compared to $M1$, as shown in Fig. 7. For the parameter b better agreement can be obtained than for a. For the nearest-neighbor general class shell of atoms b, c, b', and c' of V_2^-, rather good agreement with $G1$ can be obtained for the parameters a and b. In this comparison tensor $G1$ has been chosen as a result of the identification from motionally averaged EPR spectra, as described in Sec. IV C.

TABLE III. Hyperfine parameters a and b (MHz) for V_2^+ and V_2^-.

	V_2^+ (EPR spectrum G6)		V_2^- (EPR spectrum G7)	
Tensor	a	b	a	b
$M1$	148^{5}	28^{5}	195.2	23.3
$G1$	22.6^{37}	2.0^{37}	31.5	2.2
$G2$	19.2^{37}	0.6^{37}	19.9	3.2
$G3$	10.2^{37}	1.6^{37}	4.16	0.39

Considering only EHT results an identification with $G2$ should be likewise possible. If a factor 1.5 discrepancy for the parameter a of $M1$ is accepted, promising distortions for a simultaneous fit of the nearest-neighbor shells of V_2^- are $0.05 < EG1 < 0.1$ and $-0.05 < EG2 < 0.03$.

An identification of V_2^+ with the a_g level also gives too low parameters for the shell of atoms d and d' as compared to $M1$. For this shell and also for the nearest-neighbor general class shell no simultaneous agreement can be obtained. It is not quite possible to indicate a region of best distortions in Figs. 9 and 10, as the discrepancies for the four observed values of $M1$ and $G1$, $G2$, or $G3$ of V_2^+ will hardly be below a factor of 2 simultaneously. This happens only for distortions in the lower left quadrant of the figures.

The result of this comparison and the original comparison mentioned earlier is that the b_u level describes V_2^+ slightly better than V_2^-. The a_g level gives a poor description for both charge states, for V_2^- still worse than for V_2^+. Therefore no decisive conclusions as to the defect levels can be drawn.

From the above it is clear that EHT results cannot yet give a reliable description of a defect wave function in such detail that it can meaningfully be compared with ENDOR results. A possible improvement may be obtained by the introduction of some self-consistency by an iterative calculation which takes into account charge redistributions. Preliminary results of Weigel and Ammerlaan[30] on V_2^+ seem more promising than the EHT results reported in this section.

C. Motional effects

From the previous subsection it follows that theory for defects has not yet reached such a level that for the present results an identification of more than one shell has become possible. Besides the division in general class shells and mirror-plane class shells experimental results can give one more piece of information.

As already discussed in I at elevated temperatures motionally averaged EPR spectra can be observed as a result of a fast jump rate of the di-

vacancy between Jahn-Teller configurations with the same vacancy-vacancy axis. For V_2^- such effects are present above about 70 K. In the new higher $\bar{3}m(D_{3d})$ symmetry the two nearest-neighbor shells of the atoms d and d' and b, c, b', and c' in Fig. 1 merge together to one new six-atom shell for which a hyperfine interaction can be observed which is an average of the original hyperfine interactions. The pattern of this averaged interaction shows monoclinic I symmetry.

Observed hyperfine interactions from an EPR experiment at liquid-nitrogen temperature for a magnetic field in the [100], [111], and [011] crystallographic directions are given in Table IV. The differences in the hyperfine splittings are too small in some cases to be resolvable in EPR. Therefore the number of lines observed experimentally is smaller than corresponding to monoclinic I symmetry. Values which were calculated taking into account the anisotropic form of the g tensor are also given. Due to the y,z ambiguity in the hyperfine tensor assignments for general class shells, as mentioned in Sec. III C, two cases have to be considered. For the aim of identification the nearest-neighbor mirror-plane class shell is associated with tensor $M1$, while for the nearest-neighbor general class shell either $G1$ or $G2$ has been taken as candidate. From a comparison it is clear that $G1$ has to be identified with the nearest-neighbor general class shell in accordance with the conclusion of Watkins and Corbett.[5] The observed hyperfine axis of $G1$, moreover, has about the requisite b or c direction. From the angle γ_1 a correct bent bond angle of 109° follows, but the planes of these bent bonds are 10° out of the (011) plane. The atomic orbital which follows from the $G1$ tensor shows a surprisingly good sp^3 hybridization. This good agreement with the LCAO picture is in sharp contrast to V_2^+, where on these four atoms not the right ⟨111⟩ axial symmetry is found, whether tensor $G1$, $G2$, or $G3$ has to be assigned to that shell.

TABLE IV. Motionally averaged hyperfine interactions $\bar{A}$. Experimental values compared to theoretical ones.

$\vec{H}\|\|$	$\bar{A}_{exp}$	$\bar{A}_{calc}(M1/G1)$ Case 1	$\bar{A}_{calc}(M1/G1)$ Case 2	$\bar{A}_{calc}(M1/G2)$ Case 1	$\bar{A}_{calc}(M1/G2)$ Case 2
[100]	85±4	88.3	87.2	80.5	80.5
	85±4	86.4	86.9	79.4	79.4
[111]	103±4	104.5	100.7	92.8	92.9
	•••	80.7	82.6	75.5	75.5
	76±4	79.8	79.8	72.0	72.0
[011]	92±4	96.6	94.8	87.4	87.4
	92±4	95.2	92.7	84.1	84.2
	•••	77.0	78.2	70.8	70.8
	73±6	76.6	80.1	73.2	73.1

V. CONCLUSIONS

For the different charge states of the divacancy much information is known already, especially from EPR. From the present ENDOR measurements on the negative charge state no contradictions with the general defect model were found. The defect wave function seems similar to that for the positive charge state, except that its extent is somewhat larger. At more than 100 lattice sites the wave function could be probed. As a simple description of the defect wave function an ordinary LCAO approach turned out to be appropriate, accounting at least partially for a number of the observed properties.

For a description allowing an identification of observed interactions with lattice sites a better theory is needed. Extended Hückel theory, frequently used during the past seven years, cannot prove its promises if confronted with such a severe test for its validity as presented by ENDOR results. The identification for the two nearest-neighbor shells, earlier made from EPR, could be confirmed. For the two tensors $M1$ and $G1$, corresponding to these lattice sites, agreement with the LCAO description was very good.

ACKNOWLEDGMENT

This work received financial support from the Foundation for Fundamental Research of Matter (FOM).

*Present address: Institute for the Study of Defects in Solids, State University of New York at Albany, Albany, N. Y. 12222.

[1]J. G. de Wit, E. G. Sieverts, and C. A. J. Ammerlaan, Phys. Rev. B 14, 3494 (1976).
[2]J. W. Corbett and G. D. Watkins, Phys. Rev. Lett. 7, 314 (1961).
[3]G. D. Watkins and J. W. Corbett, Discuss. Faraday Soc. 31, 86 (1961).
[4]G. Bemski, B. Szymanski and K. Wright, J. Phys. Chem. Solids 24, 1 (1963).
[5]G. D. Watkins and J. W. Corbett, Phys. Rev. 138, A543 (1965).
[6]J. W. Corbett and G. D. Watkins, Phys. Rev. 138, A555 (1965).
[7]C. A. J. Ammerlaan and G. D. Watkins, Phys. Rev. B 5,

3988 (1972).
[8]C. A. J. Ammerlaan and A. van der Wiel, J. Magn. Reson. 21, 387 (1976).
[9]Y. H. Lee, T. D. Bilash, and J. W. Corbett, Radiat. Eff. 29, 7 (1976).
[10]L. J. Cheng, J. C. Corelli, J. W. Corbett, and G. D. Watkins, Phys. Rev. 152, 761 (1966).
[11]C. S. Chen and J. C. Corelli, Phys. Rev. B 5, 1505 (1972).
[12]H. J. Stein, Appl. Phys. Lett. 15, 61 (1969).
[13]A. H. Kalma and J. C. Corelli, Phys. Rev. 173, 734 (1968).
[14]R. C. Young and J. C. Corelli, Phys. Rev. B 5, 1455 (1972).
[15]Y. H. Lee, L. J. Cheng, J. D. Gerson, P. M. Mooney, and J. W. Corbett, Solid State Commun. 21, 109 (1977).
[16]L. C. Kimerling, in *Radiation Effects in Semiconductors, 1976*, edited by N. B. Urli and J. W. Corbett (Institute of Physics, London, 1977), p. 221.
[17]A. O. Evwaraye and E. Sun, J. Appl. Phys. 47, 3776 (1976).
[18]G. Feher, Phys. Rev. 114, 1219 (1959).
[19]E. B. Hale and R. L. Mieher, Phys. Rev. 184, 739 (1969).
[20]W. Kohn, *Solid State Physics*, edited by F. Seitz and D. Turnbull (Academic, New York, 1957), Vol. 5, p. 257.
[21]E. B. Hale and R. L. Mieher, Phys. Rev. 184, 751 (1969).
[22]E. B. Hale and R. L. Mieher, Phys. Rev. B 3, 1955 (1971).
[23]J. L. Ivey and R. L. Mieher, Phys. Rev. B 11, 822 (1975).
[24]J. L. Ivey and R. L. Mieher, Phys. Rev. B 11, 849 (1975).
[25]R. Hoffman, J. Chem. Phys. 39, 1397 (1963).
[26]R. P. Messmer and G. D. Watkins, Phys. Rev. B 7, 2568 (1973).
[27]T. F. Lee and T. C. McGill, J. Phys. C 6, 3438 (1973).
[28]C. A. J. Ammerlaan and C. Weigel, in Ref. 16, p. 448.
[29]C. A. J. Ammerlaan and J. C. Wolfrat, Phys. Status Solidi B 89, 85 (1978).
[30]C. Weigel and C. A. J. Ammerlaan, Verh. Dtsch. Phys. Ges. (VI) 13, 161 (1978); and (unpublished).
[31]E. G. Sieverts and C. A. J. Ammerlaan, in Ref. 16, p. 213.
[32]E. G. Sieverts, S. H. Muller, and C. A. J. Ammerlaan, Solid State Commun. (to be published).
[33]J. G. de Wit, thesis (University of Amsterdam, 1975) (unpublished).
[34]E. G. Sieverts, thesis (University of Amsterdam, 1978) (unpublished).
[35]R. H. van der Linde (private communication).
[36]G. D. Watkins and J. W. Corbett, Phys. Rev. 134, A1359 (1964).
[37]J. G. de Wit, C. A. J. Ammerlaan, and E. G. Sieverts, in *Lattice Defects in Semiconductors, 1974*, edited by F. A. Huntley (Institute of Physics, London, 1975), p. 178.
[38]C. Weigel, D. Peak, J. W. Corbett, G. D. Watkins, and R. P. Messmer, Phys. Rev. B 8, 2906 (1973).
[39]Y. H. Lee, N. N. Gerasimenko, and J. W. Corbett, Phys. Rev. B 14, 4506 (1976).